


RESEARCH ARTICLE | JANUARY 11 2022

Calibration of polyvinylidene fluoride (PVDF) stress gauges under high-impact dynamic compression by machine learning

Shuang Qin; Zheng Yu; Xu Zhang ; ... et. al



Journal of Applied Physics 131, 024502 (2022)

<https://doi.org/10.1063/5.0066090>



CrossMark

Articles You May Be Interested In

Wide-band electrical and electromechanical properties of polyvinylidene fluoride (PVDF) and polyvinylidene fluoride-trifluoroethylene (PVDF-TrFE) piezoelectric films using electro-acoustic reflectometry

J Acoust Soc Am (April 2023)

Underwater polyvinylidene fluoride (PVDF) acoustic sensors.

J Acoust Soc Am (April 1992)

Synthesis and crystalline properties of CdS incorporated polyvinylidene fluoride (PVDF) composite film

AIP Conference Proceedings (May 2018)



Time to get excited.
Lock-in Amplifiers – from DC to 8.5 GHz

[Find out more](#)

Calibration of polyvinylidene fluoride (PVDF) stress gauges under high-impact dynamic compression by machine learning

Cite as: J. Appl. Phys. 131, 024502 (2022); doi: 10.1063/5.0066090

Submitted: 8 August 2021 · Accepted: 2 November 2021 ·

Published Online: 11 January 2022



Shuang Qin,^{1,2} Zheng Yu,² Xu Zhang,^{2,a)} Shuqi Yang,² Wenyang Peng,² and Feng Zhao^{2,a)}

AFFILIATIONS

¹State Key Laboratory of Nonlinear Mechanics, Institute of Mechanics, Chinese Academy of Science, Beijing, 100190, China

²National Laboratory of Shock Wave and Detonation Physics, Institute of Fluid Physics, China Academy of Engineering Physics, Mianyang, Sichuan, 621900, China

^{a)}Authors to whom correspondence should be addressed: caepzx@sohu.com and ifpzf@163.com

ABSTRACT

Calibration of stress gauges is of great importance for understanding the behaviors of materials under high dynamic impacts. However, commonly used calibration models have little transferability due to ignoring the influences of the gauge parameters. In this work, we propose a systematic approach that can generate effective and transferable calibration models including multiple independent variables by machine learning. Specifically, we conduct high-impact dynamic compression experiments using polyvinylidene fluoride (PVDF) stress gauges with two different thicknesses and varying remnant polarizations at shock levels from 0.3 to 10 GPa. To best characterize the comprehensive calibration relationship, we select a set of five features (combined by strain, remnant polarization, and film thickness) by feature engineering and use Lasso with the bagging ensemble as an algorithm to train the machine learning model. For comparison, we also propose semiempirical models that calibrate PVDF gauges effectively, but without including thickness and remnant polarization. Our results show that the machine learning model is more precise and more reasonable in physics. The predicted dependences of the calibration curves on remnant polarization and film thickness by the machine learning model are qualitatively consistent with the physics scenario. This work reveals the potential of machine learning methods to improve gauge calibration for better performance and transferability. The method used in this work is applicable to the calibration of any stress gauges with multiple variables.

Published under an exclusive license by AIP Publishing. <https://doi.org/10.1063/5.0066090>

I. INTRODUCTION

Functional and precise stress gauges are prerequisites for understanding the behaviors of materials under high dynamic loading environments. For the last three decades, the gauge made of polyvinylidene fluoride (PVDF) film has been demonstrated to be effective and promising for accurate *in situ* measurement in dynamic experiments, thanks to its large piezo-stress coefficient, excellent pliability, easy integration, micrometer-scale thickness, and self-powered system.^{1–4} Recent studies reported that the piezoelectricity of PVDF can be further enhanced by adding additives like ZnO, BaTiO₃, and CNTs.^{5–8}

The mechanism of PVDF stress gauges is based on the coupling of force and electricity. Specifically, an electric field is induced by polarization imbalance in the polymers under impact stress and generates a mobile charge that can be detected by a

connected circuit system.^{9,10} The relationship between charge released from PVDF and impact stress is key to stress measurements, usually described by a calibration equation. Because the force-electricity coupling process is fast and complicated under high dynamic loading, there is no satisfying physics model that can accurately capture the relationship. Many efforts have been made to the calibration problem. Graham *et al.* used polynomial functions,¹¹ and Utriew *et al.* proposed a power equation, $\sigma = AQ^n$,¹² to empirically describe the gauge calibration up to 10 GPa. Later, Lynch and Charest derived a simple calibration function, $Q = -P_r\theta$, in which the released charge has a linear relationship with the deformation of gauge and the linear coefficient is assumed equal to the initial remnant polarization.¹³ However, later studies showed that the linear coefficient deviates from the experimental remnant polarization by 26%. Nevertheless, all these calibration

models mentioned above only apply to PVDF gauges with specific fabrication and polarization control, because parameters of PVDF films that also largely affect the calibration relationship, like geometry and polarization, are disregarded.

In this study, we aim to investigate the electrical responses of PVDF stress gauges under high-impact dynamic compression experiments and establish a transferable model to calibrate the PVDF gauges with varying gauge parameters (the remnant polarization and the film thickness) within the pressure range. Since machine learning is playing an increasing role in many fields for its ability to characterize complicated multivariate relationships,¹⁴ we apply the machine learning techniques to deal with our first-hand experimental data. Specifically, we conduct high-impact dynamic compression experiments using PVDF gauges with two different thicknesses and varying remnant polarizations at shock levels from 0.3 to 10 GPa. Two approaches are employed for the calibration task. On one hand, semiempirical models are proposed based on the approximately linear relationship between released charge and volumetric strain in PVDF. On the other hand, machine learning regression training is carefully conducted with feature engineering. In general, the trained machine learning model shows a better performance than the semiempirical model and can empirically predict calibration curves for PVDF gauges with different remnant polarizations and thicknesses. The machine learning approach used in this work is demonstrated to be effective for small datasets and can be applied to calibration for any other gauges.

II. METHODS

A. PVDF film gauge preparation

Pristine PVDF films with 20 μm and 30 μm thicknesses are commercially available (Jinzhou Kexin Inc., China). For electrical characterization, the interior electrode was formed by the magnetron sputtering technique with an area of $3 \times 3 \text{ mm}^2$ and a thickness of 0.3 μm . In our last study, the thermal cyclic poling technique has been proven a useful method to obtain stable remnant polarization of PVDF film.¹⁵ Here, we employed the same

poling method. The upper- and down-electrode structures were particularly designed and static stress of 20 MPa was applied during the poling process, in order to prevent the sample from geometric deformation, as shown in Fig. 1(a).

After the poling treatment, the rectangular pieces of the sample were cut perpendicular to the direction of polarization. A polyimide film was used as an encapsulating material, isolating the gauge from the external electric conducting environment and simultaneously providing mechanical protection. The copper foil was used as an extended electrode for its good electrical conductivity and extensibility. Each disassembled part of the entire PVDF gauge is shown in Fig. 1(b). The overlapped area of upper- and lower-interior square electrodes, $3 \times 3 \text{ mm}^2$, is the active sensing area of the PVDF stress gauge. The structure of the gauge is shown in Fig. 1(c). The total thickness of the package is about 80–100 μm .

B. Experimental setups

1. Flyer-plate-impact test

In the impact tests, the impactor and the target (or buffer layer) are made of identical material so that an equilibrium particle velocity u_p in the target is half of the impact velocity u_0 . In our tests, LY12-aluminum and C45-steel materials are selected, the dynamic mechanical properties of which have been well characterized, as listed in Table I.^{16,17} During the experiments, a flyer with a diameter of 38 mm was mounted on a sabot and then launched by either a gas-driven or explosive-driven mechanism.¹⁸ Simultaneously, the impact velocity u_0 was measured by the parallel laser light source technique. The impact stress σ on PVDF film can be determined using the impedance-match method, as given by

$$\sigma = \rho_0 u_p U_s = \frac{1}{2} \rho_0 u_0 U_s, \quad (1)$$

where ρ_0 is the initial density and U_s is the velocity of the shock wave in the target. In our experiments, the impact velocities u_0

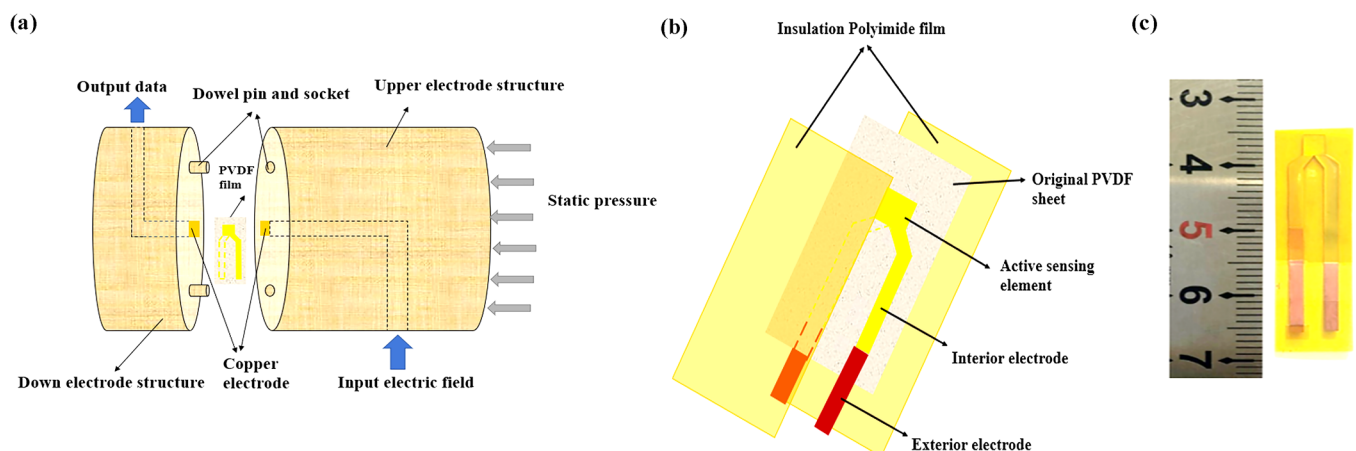


FIG. 1. Preparation of a PVDF film stress gauge. (a) An exploded schematic of the poling apparatus. (b) An exploded schematic of the gauge and (c) its actual image.

TABLE I. Characteristic parameters of the impact flyers used in this work.^{16,17}

Flyer material	ρ_0 (g/cm ³)	c_0 (km/s)	s	Longitudinal sound velocity (km/s)
LY12				
aluminum	2.785	5.328	1.338	6.360
C45 steel	7.800	4.483	1.332	5.828

covered a range of 40–150 m/s, and accordingly, the impact stress from 0.3 to 10 GPa.

The overall experimental arrangement for dynamic calibration is shown in Fig. 2. The PVDF gauge was mounted on the center of a stationary target, a 10 mm-thick cylinder with a diameter of 14 mm, and then covered by a 1 mm-thick buffer. The buffer not only protects the gauge from shear failure but also ensures that the one-dimensional planar stress wave transmits into the gauge. All these assemblies were bonded by silicone rubber. A low-loss coaxial cable transmitting electrical signals to the recording system was used.

2. Equivalent measuring circuit

Commonly, a PVDF gauge can be considered as a charge generator in parallel with capacitance and resistance, as shown in Fig. 3(a). The dashed line in the figure represents the piezoelectric sensor, in which, R_a and C_a denote its resistance and capacitance, respectively.¹⁹ A low-loss coaxial cable acting as a capacitance C_c is in parallel with the sensor. Thus, the electrical response of gauge can be expressed as

$$(C_a + C_c) \frac{dV_1}{dt} + V_1 \frac{d}{dt}(C_a + C_c) + \frac{V_1}{R_a} = \frac{dQ_1}{dt}, \quad (2)$$

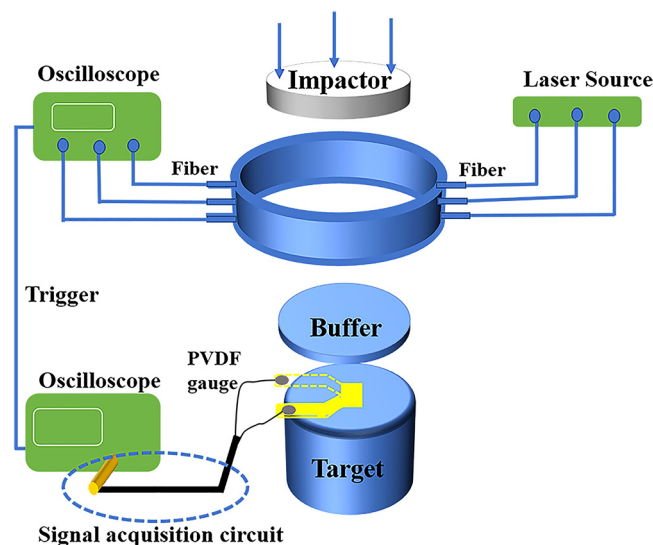


FIG. 2. A schematic diagram of the impact experimental arrangement.

where Q_1 and V_1 are the released charge and voltage, respectively. Since the resistance of the gauge R_a is rather large (about $10^{12} \Omega$) and its capacitance $C_a \approx 70$ pF is nearly constant during the impact process, the second and third terms in the LHS of Eq. (2) can be neglected. Therefore, the voltage V_1 is proportional to the released charge Q_1 . There are two common methods to record the voltage V_1 , the current-mode and the charge-mode methods. In this study, the two measurement methods were both utilized.

In the charge-mode recording circuit, the gauge is wired in parallel with a charge integrator that contains a resistance R_2 and a capacitance C_2 , as shown in Fig. 3(b). The resistance of R_2 is chosen to be 50Ω and the capacitance $C_2 = 0.1 \mu\text{F}$ to match the electrical characteristic impedance of the coaxial cable. The low-loss 2 m long coaxial cable has a capacitance $C_c = 190$ pF. During the measurement, the released charge is gathered by the capacitor C_2 and transmitted to an oscilloscope, recorded as the voltage $V_2(t)$. Since the inner resistance of the gauge is large enough, the circuit can be regarded as open, and the relation can be expressed as

$$R_2 \frac{C_1 C_2}{C_1 + C_2} \frac{dV_2(t)}{dt} + V_2(t) = V_1(t), \quad (3)$$

where C_1 is the sum of C_a and C_c ; $\tau = R_2 C_1 C_2 / (C_1 + C_2)$ is the time constant which is equal to 14.96 ns in our circuit. Integrating Eq. (3) gives

$$Q_2(t) = Q_1^0 \left(1 - \exp^{-\frac{t}{\tau}}\right), \quad (4)$$

where Q_1^0 is the initial charge stored in the gauge. Equation (4) reveals that the charge gathered by the charge integrator $Q_2(t)$ is equal to the change of charges released by the gauge. In addition, the $Q_2(t)$ can be quantitatively determined by the multiply of experimentally recorded $V_2(t)$ and C_2 .

In the current-mode method, a discharge resistance R_1 is set in series with the gauge and then connected to a recording oscilloscope, as shown in Fig. 3(c). In our test, R_1 is chosen as 50Ω and the resistance of the coaxial cable as 1.5Ω . The voltage $V_2(t)$ recorded by oscilloscope is given by

$$V_2(t) = i(t) \frac{R_1 Z}{R_1 + Z}, \quad (5)$$

where $Z = 1 \text{ M}\Omega$ is the characteristic impedance of the oscilloscope. The released charge is obtained through integration of Eq. (5) as

$$Q_1(t) = \frac{1}{R_1} \int_0^t V_2(t) dt, \quad (6)$$

where t is the experimental recording time.

C. Machine learning methods

In this paper, we apply supervised machine learning methods to characterize the calibration relation of PVDF gauge under shock compression. There are three initial input features to be considered: volumetric strain induced by shock impact (use strain instead of

Downloaded from http://pubs.aip.org/aip/jap/article-pdf/doi/10.1063/5.0066090/1650258/1024502_1_online.pdf

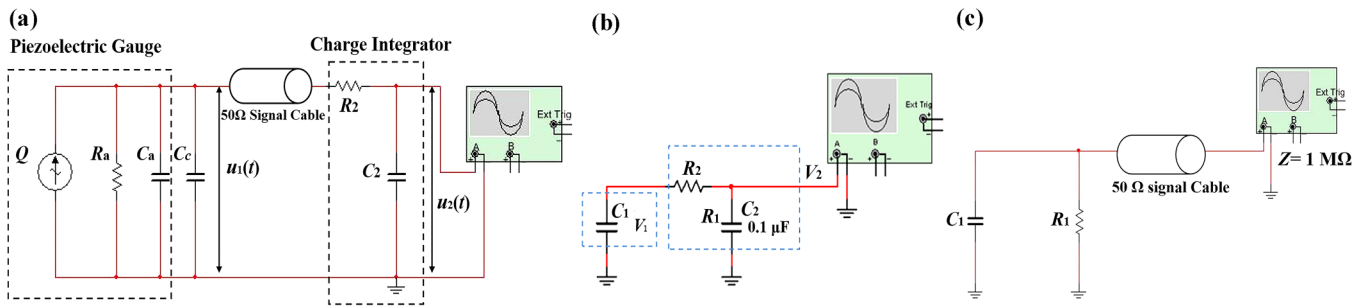


FIG. 3. Different electrical circuit systems. (a) and (b) show the charge-mode circuit and its simplified equivalent circuit. (c) shows current-mode simplified equivalent circuit.

stress because of the approximate linear relationship), remnant polarization, and initial thickness of the PVDF film. The output of the model is the charge released from the PVDF piezoelectric film under the impact, Q . The dataset includes all the experimental data in this study, 23 instances in total. We randomly chose four instances as the test data and the rest as the training data.

Because of the approximately linear relationship between volumetric strain and released charge in PVDF, we select linear regression algorithms with regularization, Lasso and Ridge, to train the model for calibration.^{20–23} Other machine learning methods, including the artificial neural network and the support vector machine, were tested as well. Without any constraints based on physical implications, these non-linear models tended to fail into overfitting and are highly unreasonable in physics due to the small dataset.²⁴

However, the remnant polarization and initial thickness would not contribute linearly to the output. Thus, polynomial and interaction terms of the initial three features were generated and used as complete inputs. Cross validation tests using ridge have shown that a polynomial degree of two is sufficient to train an optimal model, as shown in Fig. S2 of the [supplementary material](#).

To avoid overfitting, the number of the input features should be as small as possible if an adequate performance is maintained, considering the small size of the experimental data. In this case, we apply feature selection to all the features in a polynomial degree less than two. Specifically, we employ a fivefold cross validation, and in each fold, we train a Lasso model with all the features. Five features (along with a constant bias) are found to have non-zero weights (after normalization) averaged by all folds in cross validation and selected as final input features, as shown in SM. In the

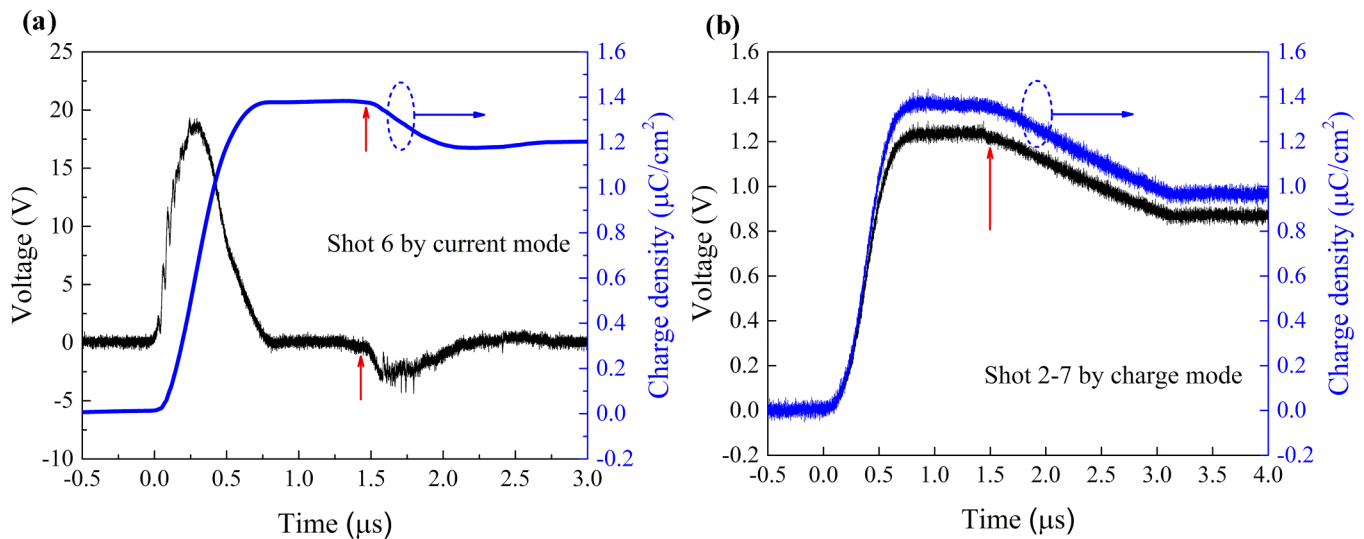


FIG. 4. PVDF gauge recording using two methods. (a) Raw recorded voltage by the current-mode method upon an impact stress of 2.516 GPa. Integrating the raw voltage can obtain the time profile of the charge. (b) Raw recorded voltage by the charge-mode method and calculated released charge curves upon an impact stress of 2.203 GPa. The arrows indicate the arrival time of the rarefaction wave at the impact surface.

Downloaded from http://pubs.aip.org/jap/article-pdf/doi/10.1063/5.0066090/1650258/1024502_1_online.pdf

end, to reduce variations caused by a small dataset, we apply the bagging ensemble with Lasso to train a final model using these five features. All the machine learning tasks in this study are performed with the Scikit-learn package for Python.

III. RESULTS AND DISCUSSION

A. Charge outputs and impact stresses of PVDF gauge

In this work, we conduct flyer-plate-impact tests using PVDF gauges and apply two experimental methods, the current mode and the charge mode, to record the released charges from the PVDF gauge on impact. Figure 4(a) shows the raw voltage recorded by oscilloscope using the current mode in one sample. The measured voltage is proportional to the rate of impact stress. The positive voltage on the left represents the loading wave upon the flyer impact and the small negative voltage on the right represents the unloading wave reflected by the back of the flyer. By integrating the voltage, we obtain the charge released from the PVDF gauge as a function of time, as shown in Fig. 4(a). The positive jump of the charge corresponds to the compression period of PVDF induced by increasing shock wave, and the plateau followed with the maximum height indicates that the PVDF gauge has reached equilibrium under the impact of the shock wave. The final released charge does not decrease to zero, indicating the failure of the PVDF gauge after high-impact stress.

The impact experiments measured by the charge-mode method are carried out on the same impact-loading facility. With a parallel capacitance, the raw voltage can directly reflect the charge released from the PVDF gauge without numerical integration. In a way similar to the current mode, the charge increases and reaches a maximum plateau before declining afterward, as shown in Fig. 4(b). In both the methods, the time duration of the recorded wave (as indicated by the arrows in Fig. 4), which starts immediately before the charge increases and ends before the charge declines, is consistent with the value calculated by theory. This suggests that the gauge can promptly detect the impact shock wave with sufficient sensitivity.

Using the two methods, we conducted a series of tests under impact stress from 0.3 to 2.5 GPa (current mode) and from 0.3 to 10 GPa (charge mode). The results are summarized in Tables II and III, respectively. The maximum charge released from PVDF gauge Q (denoted as the released charge hereinafter) is plotted as a

function of impact stress σ and volumetric strain θ (calculated from the shock adiabat relation), in Figs. 5 and 6, respectively. It can be clearly seen that the released charge increases monotonically with increasing impact stress and negative strain.

B. Calibration modeling

1. Semiempirical models

With the experimental data obtained above, we now investigate the calibration relationship between the impact stress and the charge released from PVDF. It is interesting to point out that though the charge shows a rather complex relationship with stress (Fig. 5), its relationship with volumetric strain is approximately linear (Fig. 6), which is consistent with the observation in previous experiments.^{13,25,26} Based on this, we assume $\theta = aQ + b$, where a and b are linear fitting parameters. The strain-stress relationship can be described by the Hugoniot equation

$$\sigma = -\frac{\rho_0 c_0^2 \theta}{(1 + s\theta)^2}, \tag{7}$$

where the initial density $\rho_0 = 1.8 \text{ g/cm}^3$, the Hugoniot parameters $c_0 = 2.16 \text{ km/s}$, and $s = 1.68$.¹⁹ Combining the linear relationship and Hugoniot equation, a semiempirical calibration equation of PVDF gauges can be given by

$$\sigma = -\frac{\rho_0 c_0^2 (aQ + b)}{(1 + s(aQ + b))^2}. \tag{8}$$

If the Hugoniot parameters of PVDF films are known in advance, Eq. (8) remains with only two empirical parameters, a and b . We denote this calibration equation as a two-parameter model hereinafter. Because the experimental data of PVDF gauges with different thicknesses are evidently in two lines (Fig. 6), suggesting a significant influence of PVDF film thickness on calibration, we fit the two parameters for the two thicknesses separately. The fitting parameters are summarized in Table IV and the fitting lines are shown in Fig. 6. Note that though the linear parameter a is close to the inverse of PVDF remnant polarization as mentioned in Ref. 13, this estimation should not be directly used for precise calibration in practice.

TABLE II. Experimental results using the current-mode measurements.

Shot No.	Impact velocity (m/s)	Impact stress (GPa)	Strain	Characteristics of flyer		Peak voltage (V)	Maximum charge ($\mu\text{C}/\text{cm}^2$)	Characteristics of PVDF gauge	
				Material	Dimensions (mm)			Remnant polarization ($\mu\text{C}/\text{cm}^2$)	Active sensing thickness (μm)
1	48.82	0.36	-0.038	LY12 Al	$\Phi 38 \times 3.0$	2.79	0.428	7.282	20
2	116.91	0.88	-0.079	LY12 Al	$\Phi 38 \times 3.0$	7.98	0.621	7.046	20
3	79.65	1.41	-0.111	C45 steel	$\Phi 38 \times 5.0$	11.61	1.056	7.172	20
4	80.53	1.42	-0.112	C45 steel	$\Phi 38 \times 3.0$	11.80	1.057	7.693	20
5	121.99	2.17	-0.147	C45 steel	$\Phi 38 \times 3.5$	13.60	1.196	7.218	20
6	140.95	2.52	-0.160	C45 steel	$\Phi 38 \times 3.5$	19.33	1.379	6.874	20

Downloaded from http://pubs.aip.org/aip/jap/article-pdf/doi/10.1063/5.0066090/1650258/1024502_1_online.pdf

TABLE III. Experimental results using the charge-mode method.

Shot No.	Impact velocity (m/s)	Input stress (GPa)	Strain	Characteristics of flyer		Peak voltage (V)	Maximum charge ($\mu\text{C}/\text{cm}^2$)	Characteristics of PVDF gauge	
				Material	Dimensions (mm)			Remnant polarization ($\mu\text{C}/\text{cm}^2$)	Active sensing thickness (μm)
2-1	39.48	0.35	-0.037	LY12 Al	$\Phi 38 \times 3.0$	0.35	0.39	7.356	20
2-2	107.26	0.81	-0.074	LY12 Al	$\Phi 38 \times 3.0$	0.58	0.64	7.334	20
2-3	75.98	1.34	-0.107	C45 steel	$\Phi 38 \times 10$	0.86	0.95	7.231	20
2-4	76.76	1.36	-0.108	C45 steel	$\Phi 38 \times 10$	0.94	1.04	6.867	20
2-5	117.31	2.09	-0.143	C45 steel	$\Phi 38 \times 3.5$	1.12	1.25	7.610	20
2-6	119.121	2.120	-0.145	C45 steel	$\Phi 38 \times 3.5$	1.29	1.43	7.384	20
2-7	123.708	2.203	-0.148	C45 steel	$\Phi 38 \times 3.5$	1.25	1.37	7.276	20
2-8	143.157	2.556	-0.162	C45 steel	$\Phi 38 \times 3.5$	1.34	1.49	6.730	20
3-1	47.137	0.417	-0.043	LY12 Al	$\Phi 38 \times 3.0$	0.46	0.51	7.806	30
3-2	48.434	0.429	-0.044	LY12 Al	$\Phi 38 \times 3.0$	0.59	0.67	7.791	30
3-3	126.221	0.951	-0.084	LY12 Al	$\Phi 38 \times 5.0$	0.81	0.90	7.557	30
3-4	83.384	1.476	-0.115	C45 steel	$\Phi 38 \times 5.0$	1.09	1.22	7.529	30
3-5	109.557	1.947	-0.137	C45 steel	$\Phi 38 \times 3.0$	1.37	1.52	7.878	30
3-6	129.536	2.308	-0.152	C45 steel	$\Phi 38 \times 3.0$	1.43	1.59	7.987	30
3-7	628.531	5.031	-0.228	LY12 Al	$\Phi 58 \times 5.0$	1.64	1.82	7.447	30
3-8	970.275	8.076	-0.276	LY12 Al	$\Phi 58 \times 5.0$	1.88	2.09	7.216	30
3-9	1250.441	10.734	-0.305	LY12 Al	$\Phi 58 \times 5.0$	2.36	2.62	8.287	30

If the Hugoniot parameters of PVDF film are not provided, Eq. (8) can be further modified by combining the undetermined parameters as

$$\sigma = \frac{D_1 + D_2 Q}{(1 + D_3 Q)^2}. \quad (9)$$

Here, D_1 , D_2 , and D_3 are three empirical parameters. We denote this calibration equation as a three-parameter model hereinafter. The results of the three-parameter model after fitting are summarized in Table IV and visualized in Fig. 5.

As shown in Fig. 5, the calibration curves of the two semiempirical models are in good agreement with the experimental data. The three-parameter model has a slightly smaller root mean square error (RMSE) than the two-parameter model, as shown in Table IV. This may suggest that the equation of the state of PVDF could slightly vary after polarization, or this could just be due to one more degree of freedom in the fitting. In addition, the two models with redetermined parameters can also be applied on reference experimental data under stress ranging from 2.0 to 36 GPa, as shown in the insets of Figs. 5 and 6, suggesting their applicability under a broad range of stress. In general, both the semiempirical models can well describe the charge-stress relationship of PVDF gauge under shock compression, and they have simple forms, especially compared to the polynomial calibration equations used for commercial gauges.

2. Machine learning model

Although the semiempirical models can capture the relationship between stress and released charge with sufficient accuracy, the fitting parameters in these models are dependent on the

parameters of the PVDF gauge. Considering the remnant polarization of PVDF could easily vary due to differences in fabrication and polarization processes, the transferability of the semiempirical models is limited. To solve this problem, we employ machine learning techniques to directly include the influence of remnant

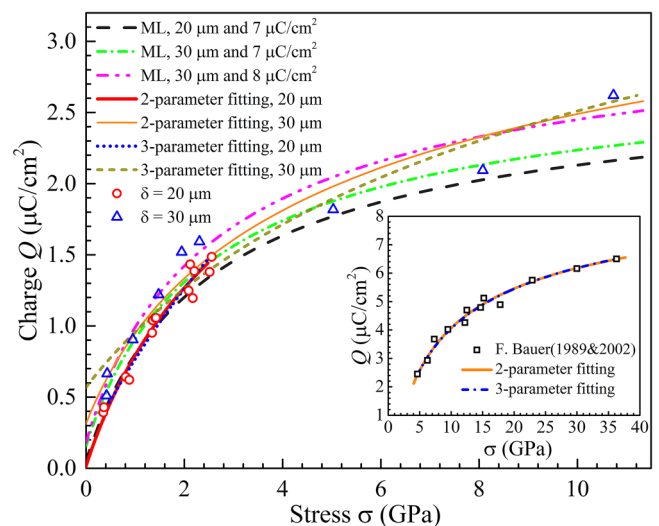


FIG. 5. Charge released from PVDF gauges as a function of impact stress. Calibration curves generated by the semiempirical models and the machine learning models are plotted, and they all agree well with the experimental data. The inset shows the application of the semiempirical calibration models on the literature experimental data.^{27,28}

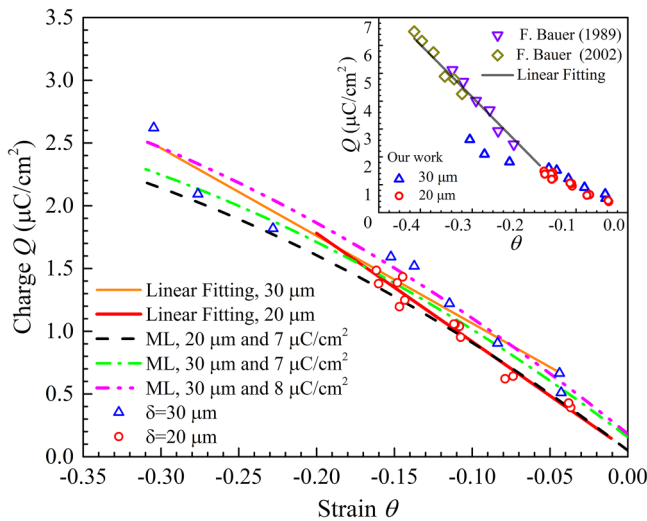


FIG. 6. Charge released from PVDF gauges as a function of volumetric strain. The semiempirical models are based on the linear relationship between charge and strain. The machine learning model, on the other hand, predicts more reasonable curves that are softer under larger strain. Data from the reference are shown in the inset.^{27,28}

polarization P_r and film thickness d . Therefore, there are three independent input features in total in this machine learning modeling. Normally, it is preferred to analyze the relationships between the inputs and the output before the modeling. However, because the three input features in this problem reveal diverse contributions, the correlations of the less significant input features (gauge parameters) with the output are difficult to observe for limited data at different volumetric strains—the dominant input feature showing an approximately linear correlation with the output, as shown in Fig. 6.

As detailed in Methods, we selected Lasso with the bagging ensemble as algorithm and a set of five features by feature engineering, θ , θ^2 , θP_r , P_r^2 , and $P_r d$, as inputs to train the machine learning model. The coefficients of the features after training are listed in Table S1 in the supplementary material. The performance of the trained model is shown in Fig. 7. The charges predicted by the model are in good agreement with the measured charges for both the 20 and 30 μm samples. R^2 of the machine learning model is 0.973 and RMSE 0.867, suggesting a slightly better performance than the semiempirical models. Note that these values are calculated based on the entire 23 instances. There are two considerations

for us to present this accuracy. (1) Because of the small test dataset and the probably included measurement errors, the test accuracy is too sensitive to the random choice of splitting. (2) This overall accuracy is for comparison with those of the semiempirical models, which are also based on the entire dataset. In the preliminary tests before applying bagging, the R^2 of the test data is higher than 0.95 in the majority of random sampling runs, suggesting the overall high accuracy is not a consequence of overfitting.

Based on the machine learning model, we now can obtain calibration curves for PVDF gauges with any remnant polarization and film thickness, as shown in Figs. 5 and 6. Note that predictions would be expected to be more appropriate with parameters within the variation range of the training data, because it is known that machine learning is better at interpolation than extrapolation. It can be seen from Fig. 5 that the predicted calibration curves are generally similar to those from the semiempirical models, while they become even softer under larger stress. This softening is associated with the predicted non-linearity in the relationship between volumetric strain and released charge, as shown in Fig. 6. The rate of charge changes by strain gradually becomes smaller under stronger impacts. This scenario is more reasonable than the linear relationship because it suggests that during high-impact compression, structural relaxation and damage that occur in the matrix and polarization gradually diminishes, besides the uniform strain effect. Evidence of this is that PVDF always cannot recover to its original state after stress is released, as shown in Fig. 4.

In addition, as shown in Fig. 5, the charges under zero-impact stress predicted by the machine learning model are all closer to zero, whereas the semiempirical curves may not. Note that we do not have such a constraint in the machine learning setting. It again demonstrates that the machine learning model better characterizes the relationship, though its R^2 and RMSE are close to those of the semiempirical models.

Furthermore, the machine learning model predicts the influence of the remnant polarization and the initial thickness of the PVDF film. As shown in Fig. 5, the released charge increases with increasing remnant polarization and the increase is more evident under large impact stress than under small stress. This is consistent with the observed approximate relationship $Q \approx P_r \theta$. On the other hand, more charge releases upon impact with a thicker PVDF film. Unlike remnant polarization, the increment of charge induced by thickness seems more uniform from small to large stress. The influence magnitude of changing thickness from 20 to 30 μm is similar to that of changing P_r from 7 to 8 $\mu\text{C}/\text{cm}^2$. The origin of the thickness effect is complicated, probably related to the structural difference between surface and bulk in the film. Based on our previous investigation, PVDF polarization during electrical poling is also

TABLE IV. Semiempirical results for PVDF gauges with two thicknesses.

Thickness (μm)	Linear or two-parameter fitting		RMSE ($\mu\text{C}/\text{cm}^2$)	R^2	Three-parameter fitting			RMSE ($\mu\text{C}/\text{cm}^2$)	R^2
	a ($\text{cm}^2/\mu\text{C}$)	b			D_1	D_2 ($\text{cm}^2/\mu\text{C}$)	D_3 ($\text{cm}^2/\mu\text{C}$)		
20	-0.111 ± 0.006	0.002 ± 0.007	0.109	0.963	-1.122 ± 0.423	3.683 ± 0.930	0.224 ± 0.109	0.088	0.973
30	-0.137 ± 0.011	0.043 ± 0.017	0.108	0.955	-1.050 ± 0.999	1.847 ± 0.923	-0.160 ± 0.005	0.099	0.942

Downloaded from http://pubs.aip.org/aip/jap/article-pdf/doi/10.1063/5.0066090/1650258/1024502_1_online.pdf

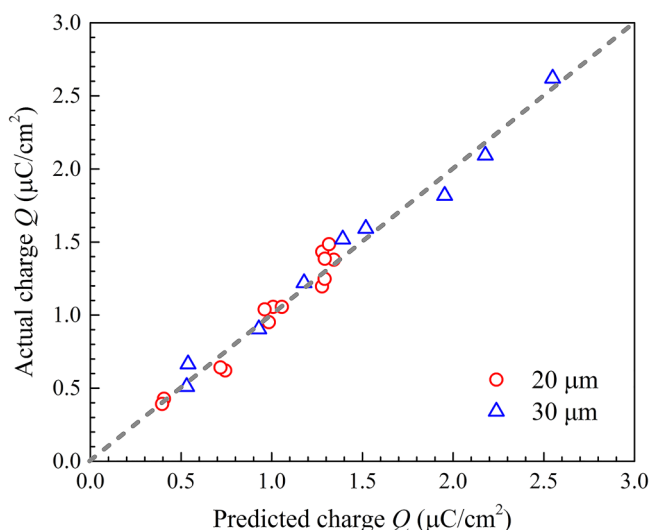


FIG. 7. Charge released from PVDF gauges predicted by the machine learning model vs actual charge measured in the experiment. The data points denoting the $20\ \mu\text{m}$ (circles) and the $30\ \mu\text{m}$ (triangles) samples both lie close to the 1:1 line, suggesting a good performance of the model.

affected by film thickness, and it suggests that the surface regions have fewer switchable dipoles than bulk.¹⁵

IV. CONCLUSION

In this work, we conduct high-impact dynamic compression experiments on PVDF stress gauges and develop a machine learning model for calibrating PVDF gauges, which is demonstrated to be more effective and transferable than the semiempirical models. The influence of the remnant polarization and the film thickness on the calibration, as well as a nonlinear relationship between volumetric strain and released charge, are not directly demonstrated due to the limited experimental data, but implied by the machine learning model. These relationships related to the fracture mechanics and the electromechanical coupling of polymers under extreme conditions are interesting topics for future atomistic and mesoscale theoretical investigations. The machine learning approach proposed in this work is suitable for learning from small datasets and can be applied to calibration in any other gauges.

SUPPLEMENTARY MATERIAL

See the [supplementary material](#) for machine learning extra details.

ACKNOWLEDGMENTS

We acknowledge the National Defense Science Foundation of China (Grant No. JSZL2016212C001), the Science Challenge Project of China (Grant No. TZ2018001 and Grant No. 2019-JCJQ-ZD-203) for supporting this work.

AUTHOR DECLARATIONS

Conflict of Interest

The authors have no conflicts to disclose.

Ethics Approval

Ethics approval is not required.

DATA AVAILABILITY

The experimental data, the trained machine learning model, and the related code are openly available in Zenodo at <http://doi.org/10.5281/zenodo.5540230>, Ref. 29.

REFERENCES

- K. S. Ramadan, D. Sameoto, and S. Evoy, *Smart Mater. Struct.* **23**, 033001 (2014).
- Y. Ting, Suprpto, A. Nugraha, C.-W. Chiu, and H. Gunawan, *Sens. Actuators, A* **250**, 129 (2016).
- X. Chen, X. Han, and Q.-D. Shen, *Adv. Electron. Mater.* **3**, 1600460 (2017).
- Y. Sato, M. Yoshida, K. Nagayama, and Y. Horie, *Int. J. Impact Eng.* **35**, 1778 (2008).
- C. Baur, J. R. DiMaio, E. McAllister, R. Hossini, E. Wagener, J. Ballato, S. Priya, A. Ballato, and D. W. Smith, *J. Appl. Phys.* **112**, 124104 (2012).
- J. Fu, Y. Hou, M. Zheng, Q. Wei, M. Zhu, and H. Yan, *ACS Appl. Mater. Interfaces* **7**, 24480 (2015).
- M. Choi, G. Murillo, S. Hwang, J. W. Kim, J. H. Jung, C.-Y. Chen, and M. Lee, *Nano Energy* **33**, 462 (2017).
- T. Sada, K. Tsuji, A. Ndayishimiye, Z. Fan, Y. Fujioka, and C. A. Randall, *J. Appl. Phys.* **128**, 084103 (2020).
- A. J. Lovinger, in *Developments in Crystalline Polymers*, edited by D. C. Bassett (Springer/Netherlands, Dordrecht, 1982), pp. 195–273.
- P. Gustavson, D. Tasker, and J. Forbes, NASA STIRcon Technical Report No. NAVSWC-TR-91-506 (1994).
- R. A. Graham, M. U. Anderson, F. Bauer, and R. E. Setchell, in *Shock Compression of Condensed Matter-1991*, edited by S. C. Schmidt, R. D. Dick, J. W. Forbes, and D. G. Tasker (Elsevier, Amsterdam, 1992), pp. 883–886.
- P. A. Urtiew, L. M. Erickson, B. Hayes, and N. L. Parker, *Combust. Explos. Shock Waves* **22**, 597 (1986).
- C. S. Lynch and J. A. Charest, in *Shock Compression of Condensed Matter-1991*, edited by S. C. Schmidt, R. D. Dick, J. W. Forbes, and D. G. Tasker (Elsevier, Amsterdam, 1992), pp. 901–904.
- Z. Yu, Q. Liu, I. Szlufarska, and B. Wang, *Phys. Rev. Mater.* **5**, 015602 (2021).
- S. Qin, X. Zhang, Z. Yu, and F. Zhao, *Polym. Eng. Sci.* **60**, 645 (2020).
- X. Zhang, J. C. Chi, and M. X. Feng, *Chin. J. High Press. Phys.* **15**, 304 (2001).
- W. Riedel, M. Wicklein, and K. Thoma, *Int. J. Impact Eng.* **35**, 155 (2008).
- S. Qin, X. Zhang, J. M. Liu, Z. Yu, F. Zhao, R. Zhang, and B. Zhong, *Propellants, Explos., Pyrotech.* **44**, 166 (2019).
- S. S. Nabatov and V. V. Yakushev, *Combust. Explos., Shock Waves* **30**, 383 (1994).
- A. E. Hoerl and R. W. Kennard, *Technometrics* **12**, 55 (1970).
- R. Tibshirani, *J. R. Stat. Soc. Ser. B Methodol.* **58**, 267 (1996).
- L. M. Ghiringhelli, J. Vybiral, S. V. Levchenko, C. Draxl, and M. Scheffler, *Phys. Rev. Lett.* **114**, 105503 (2015).
- F. Pedregosa, G. Varoquaux, A. Gramfort, V. Michel, B. Thirion, O. Grisel, M. Blondel, P. Prettenhofer, R. Weiss, V. Dubourg, J. Vanderplas, A. Passos, D. Cournapeau, M. Brucher, M. Perrot, and É. Duchesnay, *J. Mach. Learn. Res.* **12**, 2825 (2011).
- C. Cortes and V. Vapnik, *Mach. Learn.* **20**, 273 (1995).
- F. Bauer, *AIP Conf. Proc.* **78**, 251 (1982).
- F. Bauer, *AIP Conf. Proc.* **505**, 1023 (2000).
- F. Bauer, *Ferroelectrics* **92**, 29 (1989).
- F. Bauer, *AIP Conf. Proc.* **620**, 1149 (2002).
- S. Qin, Z. Yu, X. Zhang, and F. Zhao (2021). “Calibration of Polyvinylidene fluoride (PVDF) stress gauges under high-impact dynamic compression by machine learning,” Zenodo. <https://doi.org/10.5281/zenodo.5540230>